Rigorous surface enhanced Raman spectral characterization of large-area high-uniformity silver-coated tapered silica nanopillar arrays

2010 Nanotechnology 21 395701

(http://iopscience.iop.org/0957-4484/21/39/395701)

Nanotechnology **21** (2010) 395701 (9pp) doi:10.1088/0957-4484/21/39/395701

Rigorous surface enhanced Raman spectral characterization of large-area high-uniformity silver-coated tapered silica nanopillar arrays

Manas R Gartia[1,3], Zhida Xu[1], Elaine Behymer[2], Hoang Nguyen[2], Jerald A Britten[2], Cindy Larson[2], Robin Miles[2], Mihail Bora[2], Allan S-P Chang[2], Tiziana C Bond[2,4] and G Logan Liu[1,4]

[1] Micro and Nanotechnology Laboratory, Department of Electrical and Computer Engineering, University of Illinois at Urbana-Champaign, USA
[2] Center of Meso, Micro and Nano Scale Technology, Lawrence Livermore National Laboratory, USA
[3] Department of Nuclear, Plasma and Radiological Engineering, University of Illinois at Urbana-Champaign, USA

E-mail: loganliu@illinois.edu and bond7@llnl.gov

Received 21 May 2010, in final form 12 August 2010
Published 1 September 2010
Online at stacks.iop.org/Nano/21/395701

Abstract
Surface enhanced Raman spectroscopy (SERS) has been increasingly utilized as an analytical technique with significant chemical and biological applications (Qian *et al* 2008 *Nat. Biotechnol.* **26** 83; Fujita *et al* 2009 *J. Biomed. Opt.* **14** 024038; Chou *et al* 2008 *Nano Lett.* **8** 1729; Culha *et al* 2003 *Anal. Chem.* **75** 6196; Willets K A 2009 *Anal. Bioanal. Chem.* **394** 85; Han *et al* 2009 *Anal. Bioanal. Chem.* **394** 1719; Sha *et al* 2008 *J. Am. Chem. Soc.* **130** 17214). However, production of a robust, homogeneous and large-area SERS substrate with the same ultrahigh sensitivity and reproducibility still remains an important issue. Here, we describe a large-area ultrahigh-uniformity tapered silver nanopillar array made by laser interference lithography on the entire surface of a 6 inch wafer. Also presented is the rigorous optical characterization method of the tapered nanopillar substrate to accurately quantify the Raman enhancement factor, uniformity and repeatability. An average homogeneous enhancement factor of close to 10^8 was obtained for benzenethiol adsorbed on a silver-coated nanopillar substrate.

(Some figures in this article are in colour only in the electronic version)

1. Introduction

The extensive use of Raman spectroscopy as a bio-molecule detection tool is still restricted due to its weak sensitivity as compared to other scattering mechanisms (roughly only 1 in 10^8 photons ends up in Raman scattering) [8] and also due to the typical lower scattering cross-section of the Raman process ($\sim 10^{-30}$ cm^2) which is around 15 orders of magnitude lower than fluorescence emission [9]. In order to get detectable Raman scattering it is necessary to use an array of filtering techniques or to enhance the Raman scattering process. The latter can be achieved using surface enhanced Raman spectroscopy (SERS). In 1997, Kneipp *et al* [10] reported that SERS might be capable of single-molecule detection. Nie and Emory [11] also independently confirmed the findings and proposed the concept of 'hot particles' which are capable of producing very high enhancement ($\sim 10^{14}$), which can be used for single-molecule detection. The single-molecule SERS experiment by Nie and Emory [11] was done with dry silver colloidal particles with Rhodamine 6G

[4] Author to whom any correspondence should be addressed.

molecules, whereas Kneipp *et al* [10] did the experiments with crystal violet dye molecules in aqueous colloidal silver solution. The concentrations in both the cases were ultralow so that there are a small number of analytes per colloid, typically ∼0.1 molecule/colloid. The single-molecule nature of the signals was inferred from the ultralow concentration of the sample. Because of low analyte concentration, it was statistically suggested that there cannot be more than about one molecule per colloid or an average of one molecule in the scattering volume if several colloids are present. So, if any SERS signal is observed then it must originate from a single molecule. In the context of the single-molecule SERS experiment, it should be noted that the experiments were performed with very strong dye molecules (Rhodamine 6G (R6G) and crystal violet), which inherently have Raman cross-sections much larger than 10^{-30} cm^2 due to resonance effects (e.g. isolated R6G has a resonance Raman cross-section of $\sim 10^{-24}$ cm^2 sr^{-1}). Hence, single-molecule detection of R6G can be achieved even with a surface enhancement factor of about 10^{10}. However, above these values SERS active substrate preparation processes are hampered by the need to use a more time consuming bio-conjugation process of the molecule to the colloids. The inherent statistical distribution of colloids in the solution also makes it difficult to get uniform and reproducible detection (and enhancement factor) consistently.

On the other hand, the dramatic development of nanotechnology opens the possibilities of new SERS substrate design and fabrication. One of the many approaches that has been tried includes micro- or nanoscale 'roughening', either in the form of electrochemical texturing of a surface before metal sputtering [12], or as a metal colloid either bonded to a surface [13, 14], or in close proximity to a surface. In the last technique, the sample molecules are placed onto a sol–gel matrix of silver particles coating the inside of a glass vial—the molecules are injected into the vial in solution, permitting SERS of those which then leave the solution and embed themselves into the matrix [15, 16]. The nanoscale approaches also include (self-) assemblies of latex nanoparticles, which, when electroplated and subsequently dissolved away, leave behind nanovoids or nanoholes (ordered and irregular, respectively) [17, 18]. This popular nanosphere lithography technique has also been applied to create ordered 2D nanoparticle arrays (often called a Fischer pattern), typically using a colloid crystal as evaporation or etching mask [19–21]. In addition, the straightforward binding of molecules to single metal nanoparticles has also been reported to have yielded Raman signal enhancement, leading to the detection of single-molecule Raman spectra [10, 11, 22, 23]. In general, the reported signal enhancements are as much as six orders of magnitude or more. However, a mature and sizable level of commercial success is yet to be achieved by these technologies. In spite of having a fairly reliable manufacturing process in replicating the surfaces, the level of enhancement measured across a single surface remains unacceptably inconsistent. Enhancement is observed only at so-called 'hot spots', regions where the Raman signal is very high, while neighboring regions might exhibit little or even no significant signal enhancement. This situation is exacerbated further by an inconsistency of performance between different but essentially identical substrates [24]. Overall, these two aspects together effectively have prevented SERS from being widely recognized as a quantifiable spectroscopic technique [25].

In this paper, we describe a rigorous SERS characterization experiment with a substrate made up of silver-coated silica nanopillar arrays produced by large scale laser interference lithography and following metal deposition. The pillars have shown to have great tunability potential [26] and with an adiabatic taper of ∼25° offer the additional advantage of nano-focusing and impedance matching [27, 28]. This low cost yet highly uniform SERS substrate is field deployable, robust and designed to be a reproducible detection platform for bio-molecules. Here, we describe the optical characterization experiments with the standard Raman molecule benzenethiol (C_6H_6S), due to its ready nature to form a uniform self-assembled monolayer (SAM) on noble metal material such as silver and gold [29, 30] (which are also the preferred material coatings for tapered nanopillar SERS substrates because of their optimal plasmon properties in the visible range) [26].

2. SERS substrate preparation

The nanopillar SERS substrates were prepared using the following method. Firstly a 4 inch diameter (also performed with a 6 inch diameter) silicon dioxide wafer is coated with an average 0.45 μm thick photoresist and then exposed by 413 nm wavelength laser interference illumination with a dose of ∼40 mJ cm^{-2}. After the photoresist development, the wafer is covered by a uniform array of nanoscale circular photoresist mask of 150 nm in diameter and 350 nm in spacing distance [31]. Secondly the wafer is subject to ion milling deep reactive ion etching by using a highly directional Bosch process. The unprotected silicon dioxide area was etched down for 500 nm leaving behind the array of silicon dioxide nanopillars. As there is also the lateral etching to the photoresist-protected area, or 'undercut', although at a much slower etch rate, the silicon dioxide nanopillars are tapered and have sharp tips at the top. Finally after completely stripping the photoresist, the wafer covered with nanopillar array structures on the entire surface was subject to metal deposition.

In order to make the nanopillar surfaces SERS active, e-beam evaporation of an 80 nm thick film of silver onto the nanopillar surface was performed. The film was deposited at a rate of 0.1 nm s^{-1}, with no heating or cooling applied to the substrate during deposition. To make the deposition uniform, the sample was kept on a hemispherical mounting rotating at 50 rpm (revolution per minute) inside the e-beam chamber. Figures 1(A) and (B) show the scanning electron microscope image of the LLNL (Lawrence Livermore National Laboratory) nanopillar SERS substrate before depositing silver and after being coated with 80 nm of silver respectively.

After the deposition, the silver-coated LLNL substrates were then functionalized with a SAM of benzenethiol using an earlier described procedure [32]. The substrates were submerged in 4 mM solutions of benzenethiol made with ethanol for 1 h and then gently rinsed in neat ethanol for 1 min, followed by drying under a stream of nitrogen.

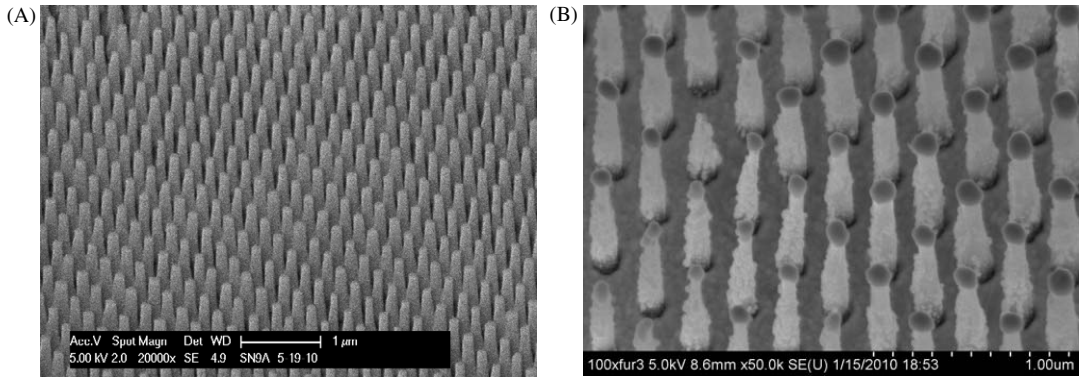

Figure 1. (A) SERS substrate before deposition of silver and (B) side view (25°) of SERS substrate after depositing 80 nm of silver.

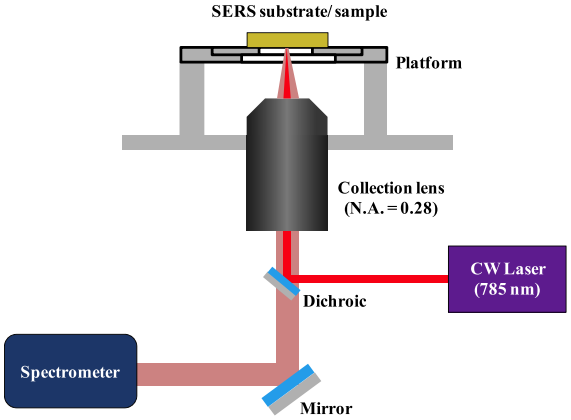

Figure 2. Schematic of SERS experimental setup.

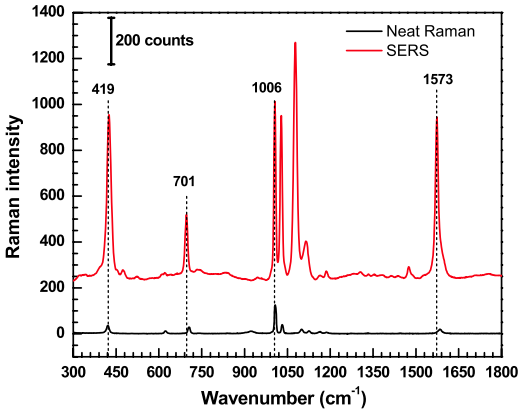

Figure 3. Normal Raman and SERS spectrum of benzenethiol, obtained using 35.0 mW of 785 nm pump power and 1 s integration time.

3. Experimental setup

The normal Raman and the SERS spectra of benzenethiol were measured in a Raman spectrometer system with 785 nm laser excitation. The system comprised a semiconductor 785 nm CW diode laser, a microscopy system and a thermoelectric cooled (−80 °C) CCD camera (PIXIS-400, Princeton Instruments). The spectral resolution of the spectrometer was approximately 1.5 cm^{-1} in the near-infrared range. A 10× microscope objective lens (Mitutoyo infinity-corrected long working distance objectives, Edmund Optics, Part No. NT46-144) with an effective focal length of 20 mm and diameter of 24 mm was used to focus the excitation laser beam onto the sample and to collect the backscattered radiation for input into the Raman spectrometer. Figure 2 shows the schematic of the SERS experimental setup.

4. Normal Raman scattering cross-section

Benzenethiol (>99% purity) was purchased from Sigma-Aldrich. About 0.5 ml of neat benzenethiol was poured into a PDMS cell of thickness 0.5 mm to perform the normal Raman spectra. Figure 3 shows the background corrected RS spectrum of neat benzenethiol obtained using 35.0 mW of 785 nm CW laser and 1 s integration time in a 20 μm spot size. Consistent with earlier reported findings [32–38] strong Raman bands are observed at 419 ($\beta_{CCC} + \nu_{CS}$), 621 ($\beta_{CCC} + \nu_{CS}$), 704 ($\beta_{CCC} + \nu_{CS}$), 919 (β_{SH}), 1006 (β_{CCC}), 1032 (β_{CH}), 1099 ($\beta_{CCC} + \nu_{CS}$), 1125 (β_{CH}), 1164 (β_{CH}), 1187 (β_{CH}) and 1584 (ν_{CC}) cm^{-1}. Here, β and ν indicate the in-plane bending and the stretching modes respectively. The full width at half maximum (FWHM) of the fully resolved 1584 cm^{-1} band is 25 cm^{-1}. The normal Raman intensity was calculated by integrating the area under the 1584 cm^{-1} band and was found to be 124 counts.

5. Surface enhanced Raman scattering cross-section

The SERS spectrum for the monolayer of benzenethiol on LLNL nanopillar substrate with an 80 nm silver coating is shown in figure 3. This is a typical plot of SERS spectrum averaged over four measurements at the same spot. As seen from figure 3, it is clear that the normal Raman spectrum and SERS spectrum differ in their Raman intensities bands which means that the enhancement factors are not the same for all the Raman bands. Also the 919 cm^{-1} (β_{SH}) band disappeared from the SERS spectra confirming that the benzenethiol is bonded to the silver surface through the thiol bond. The shifts in Raman bands are consistent with the observations of

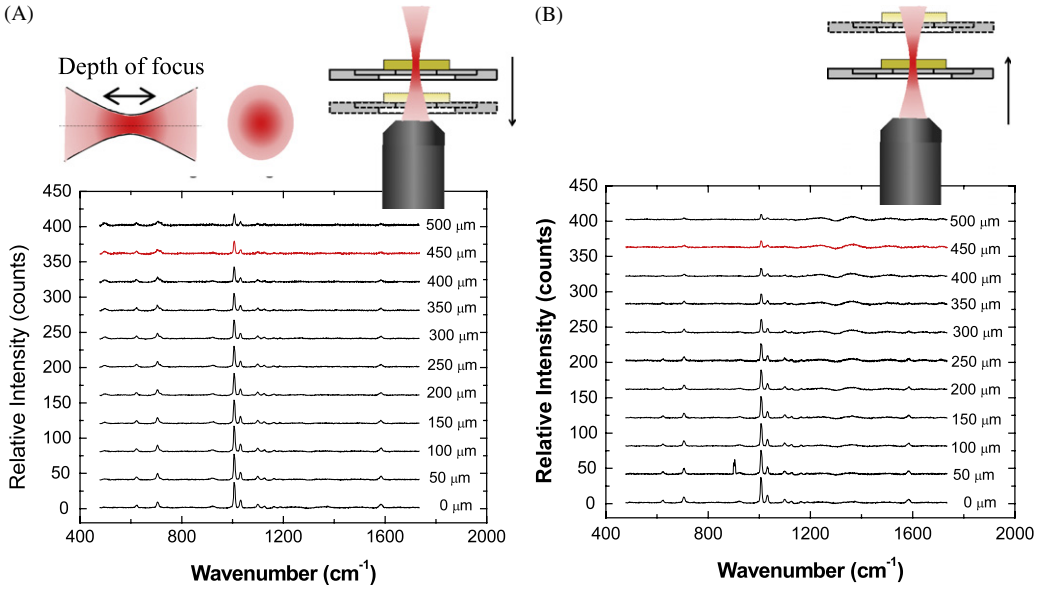

Figure 4. (A) Raman intensity plot when the stage is moving in the down direction relative to the equilibrium stage position and (B) Raman intensity plot when the stage is moving in the up direction relative to the equilibrium stage position.

Joo *et al* [33] and Roshan *et al* [32]. We have considered the Raman intensities of the 1584 (ν_{CC}) cm^{-1} band (C–C stretching mode) to calculate the approximate enhancement factor because of its regular appearance in both the normal Raman and the SERS spectra. It should be noted that there is a slight shift in the Raman band for the normal Raman spectrum which occurs at 1584 cm^{-1} as compared to that of the SERS spectrum which occurs at 1573 cm^{-1}. This observation is quite similar to that reported by Roshan *et al* [32]. The full width at half maximum (FWHM) of the fully resolved 1573 cm^{-1} band is 12 cm^{-1}. The SERS intensity was calculated by integrating the area under the 1573 cm^{-1} band and was found to be 44 593 counts.

6. Raman scattering length

The Raman scattering length is an important factor in calculating the average enhancement factor of the SERS substrate. For characterizing the Raman scattering length, the neat benzenethiol was carefully mounted in a PDMS cell with a depth of 0.5 mm. The PDMS cell depth was chosen based on the knowledge of depth of focus of the laser system we are using (rule of thumb says the depth of cell should be close to or smaller than the depth of focus). The Raman spectrum was taken when the stage was at the equilibrium position (focused position). Subsequently the stage was moved up and down relative to the equilibrium position. Finally, the scattering length was deduced as the length at which the Raman intensity reduced by a factor half of 1/e as compared to the initial equilibrium position intensity. Figures 4(A) and (B) show a series of Raman spectra acquired at a regular distance interval of 50 μm covering the total depth of the cell and for the cases when the stage is moving up and down relative to the equilibrium position respectively.

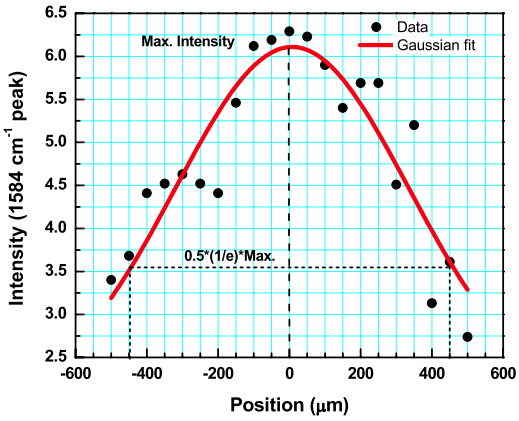

Figure 5. Variation of Raman intensity of 1584 cm^{-1} band (obtained using 35.0 mW of 785 nm pump power and 1 s integration time) with distance when the stage is moving in the up and down directions relative to the equilibrium stage position.

The variation of Raman intensity as a function of position compared to equilibrium position has also been plotted. Figure 5 shows the variation of Raman intensity of the 1584 cm^{-1} band as a function of position when the stage is moving in the down and up directions. As shown in the figure, the intensity keeps on reducing while moving away from the focused position. From the study, it was found that the scattering length for our instrument is 450 μm (distance at which the intensity falls to 50% of the 1/e value of the maximum).

7. Area multiplication factor

Due to the creation of nanopillars, the effective surface area available for the formation of the monolayer of benzenethiol is increased as compared to a flat surface. This factor has

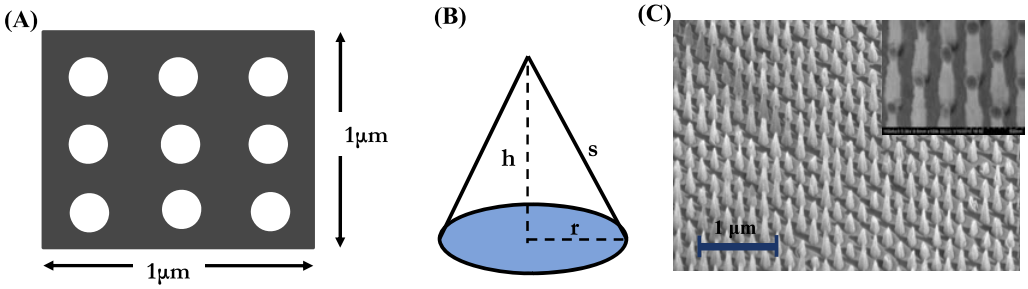

Figure 6. (A) Schematic of average number of pillars per unit area, (B) assumed structure for the nanopillar, (C) SEM of LLNL nanopillar substrate with 80 nm silver deposited pillar shown in the inset.

to be taken into consideration while calculating the average enhancement factor for the SERS substrate. With a special deposition technique with hemispherical mounting and having the sample at a tilt angle of 25° as well as rotation of 50 rpm, we successfully deposited silver on the side wall of tapered pillars (as shown in the SEM in the inset in figure 6(C)). The schematics of nanopillar distribution and shape of the pillar are shown in figures 6(A) and (B) respectively. Considering a pillar radius of 75 nm and pillar height of 750 nm, m was calculated to be 2.44 using the relation

$$m = \frac{[A_{1\times1} - 9\pi r^2 + 9A_{\text{cone}}]}{A_{1\times1}}.$$

8. Enhancement factor

The absolute Raman cross-section of benzenethiol has already been calculated by Roshan *et al* [32]. Hence, instead of calculating the absolute Raman cross-section, here focus has been shifted to characterizing the effectiveness of the current SERS substrate, prepared using a novel laser interference technique, by calculating the enhancement factor (EF). As described in detail by Roshan *et al* [32], the expression for the enhancement factor can be given as:

$$EF = \frac{I_{\text{SERS}}}{I_{\text{RS}}} \frac{N_{\text{RS}} L}{N_{\text{SERS}} m} \frac{1}{n^2}$$

where I_{SERS} and I_{RS} are the Raman intensity from SERS substrate and neat benzenethiol respectively, N_{RS} is the molecular density of the benzenethiol, N_{SERS} is the areal density of benzenethiol on a flat surface, L is the Raman scattering length, m is a multiplier that accounts for the increased surface area of the nanostructured surface and n is the refractive index of benzenethiol. Substituting the values of 1.56 for n [39], 44 593 for I_{SERS}, 3.3×10^{14} cm^{-2} for N_{SERS}, 124 for I_{RS}, and 5.9×10^{21} cm^{-2} for N_{RS} [32], 0.045 cm (450 μm) for L, 2.44 for m, we obtain a value of average enhancement factor of $EF_{\text{ave}} = 0.4873 \times 10^8$ for our tapered nanopillar SERS substrate.

9. Repeatability of the SERS experiment

The repeatability and uniformity of the SERS signal across the SERS substrate is an important parameter for designing a robust SERS substrate. The robustness of the LLNL nanopillar SERS substrate was characterized by taking several SERS spectra by scanning the laser across the substrate. The SERS substrate was mounted on a motorized platform which was controlled by the LABVIEW program. The sample was scanned for a total of 57 data points, and at each point the measurement was repeated four times (total sample space of 228 points). A typical 5 × 5 array 2D scanning result is reported in figure 7(A). The scanning scheme is given in the inset. The SERS peak intensity distribution for a typical peak (1573 cm^{-1}) obtained using 35.0 mW of 785 nm pump power and 1 s integration time is reported in figure 7(B). The surface plot showing the 2D scanning result has been shown in figure 7(C). To confirm the robustness of the substrate the intensity distribution of the SERS spectra was also calculated for many other peaks (1573, 1099, 1006, 704 and 419 cm^{-1}) and shown in figure 7(D). The distributions for all the peaks are found to be following a Gaussian distribution. However, the 1573 cm^{-1} peak, which was used for calculating the SERS enhancement factor, was found to be fairly uniform. Finally, figure 8 shows the probability distribution of the enhancement factor calculated for the entire substrate. This follows a Gaussian distribution with a maximum enhancement factor of 0.487×10^8 and an average enhancement factor of 0.14×10^8. This showed the uniformity of the SERS substrate and confirmed that the LLNL nanopillar SERS substrate is fairly robust.

10. Discussion on the nanopillar array SERS substrate

In general, two mechanisms are responsible for the SERS enhancement: the electromagnetic (EM) effect and the chemical or charge transfer (CT) effect. The EM mechanism in particular is related to the morphology of the substrate and hence relevant to the current discussion.

In the EM mechanism, surface plasmons on the surface of the metal (nanostructure) are excited by incident laser light. It should be noted that the electromagnetic fields can be strongly enhanced in the presence of surface plasmons only if certain resonance conditions are fulfilled. Finally, the product of the enhancement of the incident laser field and the scattered Raman yields the observed overall electromagnetic

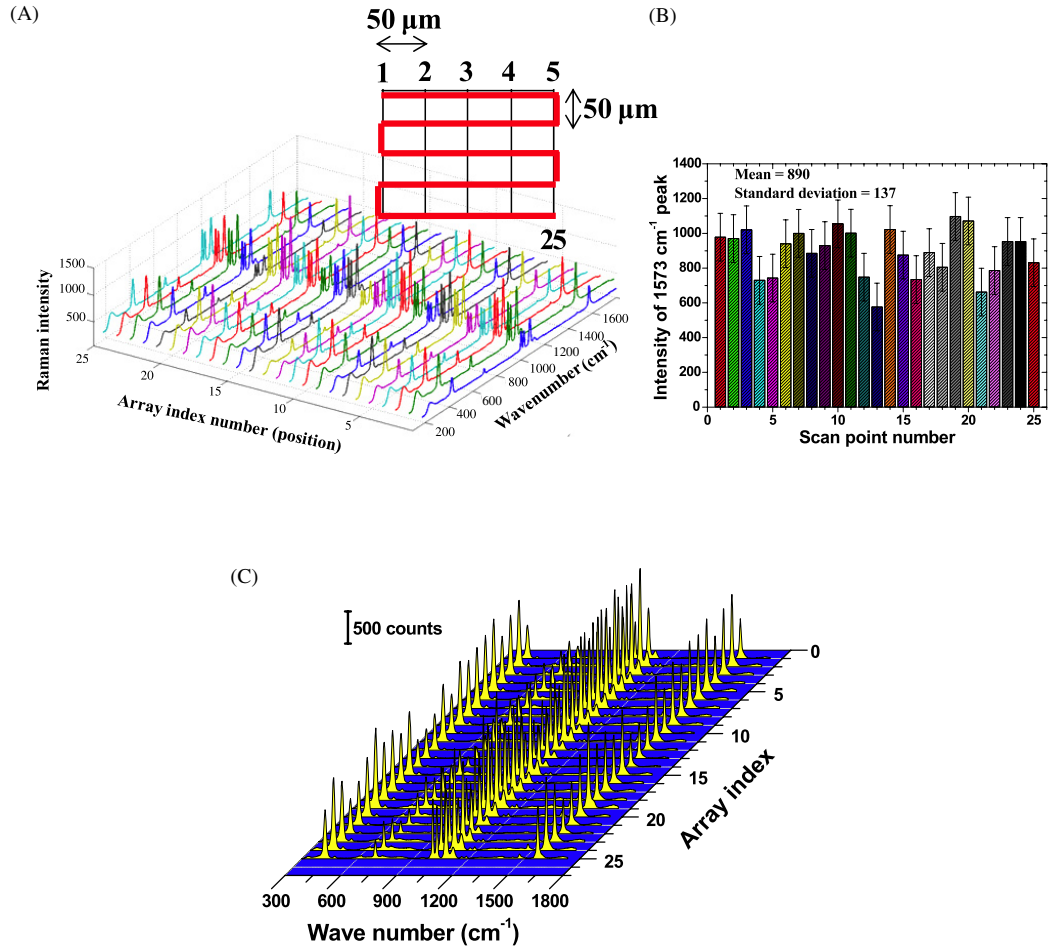

Figure 7. (A) 2D scanning SERS data for the LLNL nanopillar substrate obtained using 35.0 mW of 785 nm pump power and 1 s integration time. (B) 2D scanning SERS intensity distribution for 1573 cm^{-1} Raman peak-distribution (mean of 890 ± 137). (C) Surface plot of 2D scanning SERS data for the LLNL nanopillar substrate obtained using 35.0 mW of 785 nm pump power and 1 s integration time. (D) SERS intensity distribution for various Raman peaks (1573, 1099, 1006, 704 and 419 cm^{-1}) and the histogram showing the number of occurrences of particular intensity values.

SERS effect. It is also well known from the TERS (tip enhanced Raman spectroscopy) experience that a sharp metal tip can highly confine the electromagnetic field at the apex of a tip (due to an electrostatic lightning rod effect as a result of the shape of the tip) [40]. The high electromagnetic field at the tip is also due to the surface plasmon resonances which correlate the wavelength of the excitation source and the actual tip geometry. In addition it was also predicted theoretically that optical energy can be nano-focused in a tapered plasmonic waveguide [27]. The enhanced electromagnetic field relies on the concentration of optical energy in a localized spot (so-called 'hot spot'). In nanopillar arrays this can be done by exciting the surface plasmon polaritons (SPPs) propagating toward a tip of a tapered dielectric coated metal array [28]. This propagation of SPPs undergoes a rapid adiabatic slowing down and asymptotic stopping at the tip due to the boundary condition. This phenomenon leads to a giant concentration of energy on the nanoscale. In a sense the SPPs are adiabatically transformed into localized surface plasmons (SPs) [27]. Moreover the tapered nanopillar array could potentially provide a better antenna effect to effectively collect excitation energy and emit Raman scattering light.

It is believed that the gap between nanopillars can contribute additional localized surface plasmon resonance, thereby enhancing the electromagnetic field [41, 42]. It is also well known that coupling of propagating surface plasmon polariton (PSSP) to light is possible by creating a grating like structure on the surface (nanopillar arrays). This is because of relaxation of the conservation of momentum restriction or so-called 'breaking the translational invariance' [43].

Preliminary optical characterization on a Zeiss reflection microscope for the nanopillar substrate showed a reflectance dip near 700 nm (figure 9). A similarly strong absorption peak near 700 nm can be seen in the extinction spectra (figure 10). Due to strong dependence of the SERS enhancement on the overlap between the incident light and the plasmon resonance, we have used 785 nm laser light for the excitation of the surface plasmon in our experiment. Further modeling and characterization studies are ongoing, which will help in deciphering what kind of electromagnetic distribution these resonances have.

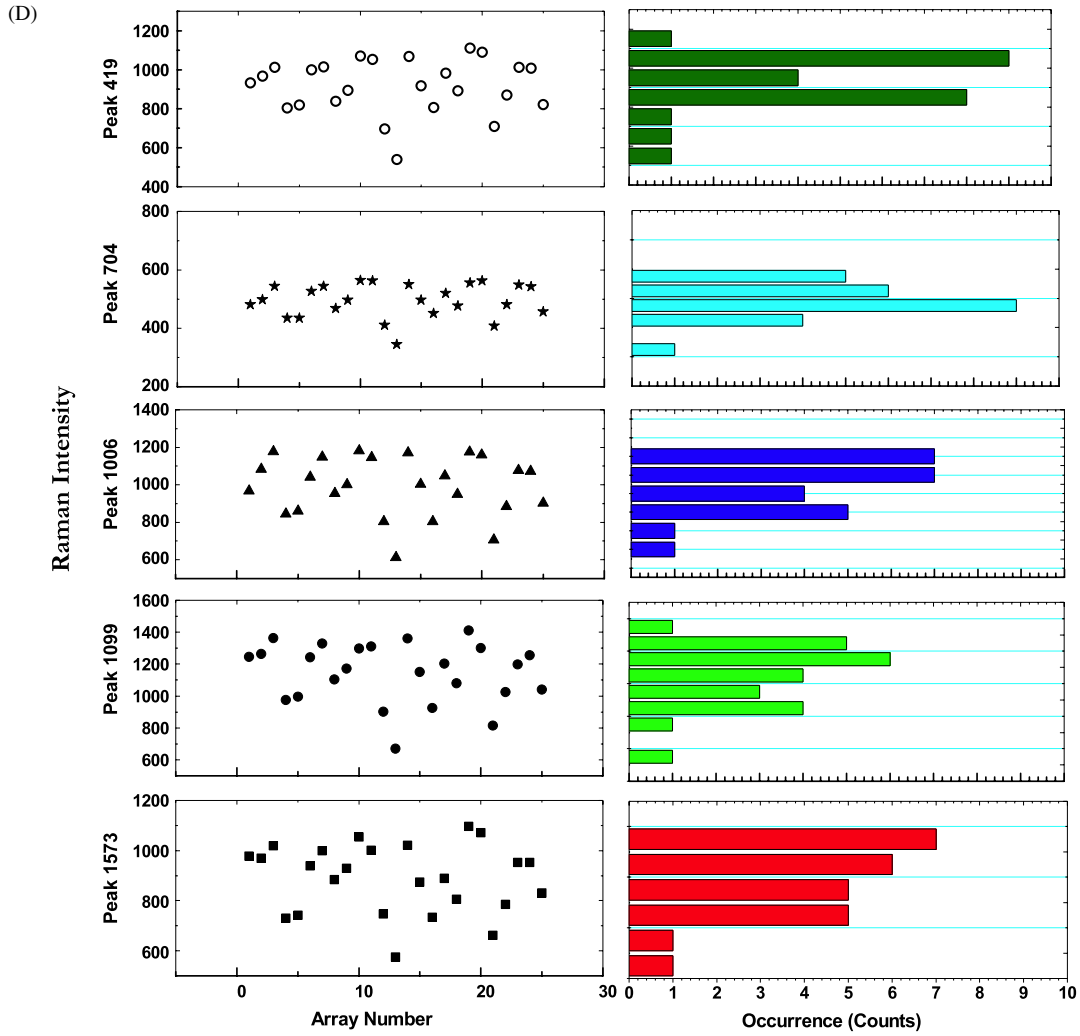

Figure 7. (Continued.)

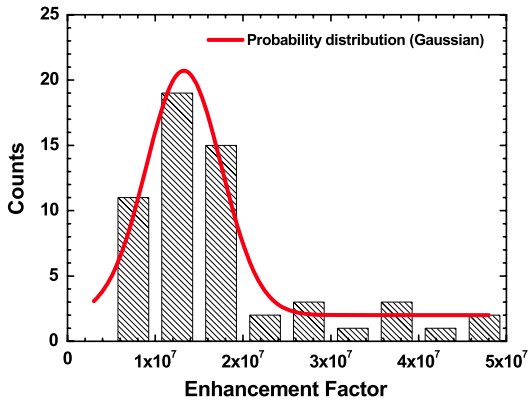

Figure 8. Probability distribution showing the enhancement factor calculated for the entire substrate.

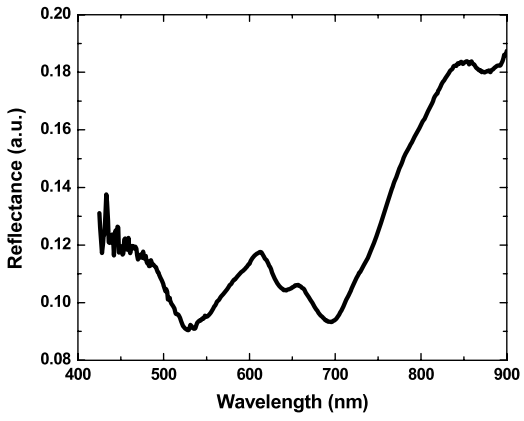

Figure 9. Reflectance spectra of the nanopillar SERS substrate.

11. Conclusion

In conclusion, we have produced a highly ordered Ag coated nanopillar SERS substrate using a novel laser interference nano-lithography technique. A uniform enhancement of $\sim 0.5 \times 10^8$ (with peaks at 0.14×10^8) has been demonstrated using a SAM of benzenethiol on the SERS substrate. From the results, it can be inferred that the laser interference based approach is capable of fabricating large-area uniform SERS active substrates. This simple and straightforward method for

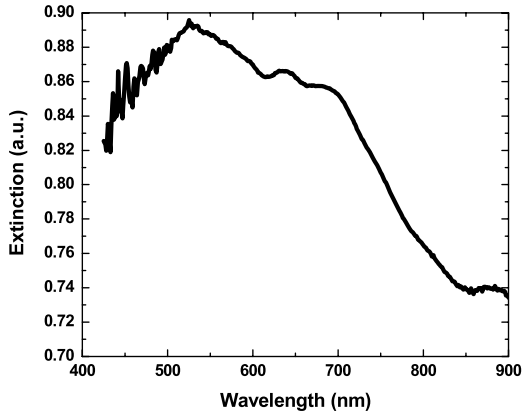

Figure 10. Extinction spectra of the nanopillar SERS substrate.

fabricating SERS substrates offers considerable potential for the batch fabrication as well as commercialization of such robust substrates, and hence opens the door for practical sensor chips based on SERS.

Acknowledgments

This work was supported by Lawrence Livermore National Laboratory under Contract No. AC52-07 NA27344. We also acknowledge support by the Defense Advanced Research Projects Agency (DARPA).

References

[1] Qian X, Peng X H, Ansari D O, Goen Q Y, Chen G Z, Shin D M, Yang L, Young A N, Wang M D and Nie S 2008 *In vivo* tumor targeting and spectroscopic detection with surface-enhanced Raman nanoparticle tags *Nat. Biotechnol.* **26** 83

[2] Fujita K, Ishitobi S, Hamada K and Smith N I 2009 Time-resolved observation of surface-enhanced Raman scattering from gold nanoparticles during transport through a living cell *J. Biomed. Opt.* **14** 024038

[3] Chou I H, Benford M, Beier H T, Coté G L, Wang M, Jing N, Kameoka J and Good T A 2008 Nanofluidic biosensing for beta-amyloid detection using surface enhanced Raman spectroscopy *Nano Lett.* **8** 1729

[4] Culha M, Stokes D, Allain L R and Vo-Dinh T 2003 Surface-enhanced Raman scattering substrate based on a self-assembled monolayer for use in Gene Diagnostics *Anal. Chem.* **75** 6196

[5] Willets K A 2009 Surface-enhanced Raman scattering (SERS) for probing internal cellular structure and dynamics *Anal. Bioanal. Chem.* **394** 85

[6] Han X X, Zhao B and Ozaki Y 2009 Surface-enhanced Raman scattering for protein detection *Anal. Bioanal. Chem.* **394** 1719

[7] Sha M Y, Xu H, Natan M J and Cromer R 2008 Surface-enhanced Raman scattering tags for rapid and homogeneous detection of circulating tumor cells in the presence of human whole blood *J. Am. Chem. Soc.* **130** 17214

[8] Jarvis R M and Goodacre R 2004 Discrimination of bacteria using surface-enhanced Raman spectroscopy *Anal. Chem.* **76** 40

[9] Vo-Dinh T, Allain L R and Stokes D L 2002 Cancer gene detection using surface-enhanced Raman scattering (SERS) *J. Raman Spectrosc.* **33** 511

[10] Kneipp K, Wang Y, Kneipp H, Perelman L T, Itzkan I, Dasari R R and Feld M S 1997 Single molecule detection using surface-enhanced Raman scattering (SERS) *Phys. Rev. Lett.* **78** 1667

[11] Nie S and Emory S R 1997 Probing single molecules and single nanoparticles by surface-enhanced Raman scattering *Science* **275** 1102

[12] Murray C A, Allara D L and Rhinewine M 1981 Silver molecule separation dependence of surface enhanced Raman scattering *Phys. Rev. Lett.* **46** 57

[13] Dick L A, Mcfarland A D, Haynes C L and Van Duyne R P 2002 Metal film over nanosphere (MFON) electrodes for surface-enhanced Raman spectroscopy (SERS): improvements in surface nanostructure stability and suppression of irreversible Loss *J. Phys. Chem.* B **106** 853–60

[14] Vo-Dinh T 1995 SERS chemical sensors and biosensors: new tools for environmental and biological analysis *Sensors and Actuators* B **29** 183–9

[15] http://www.rta.biz/Content/SERV_Vials.asp

[16] Farquharson S, Inscore F E and Christesen S 2006 Detecting chemical agents and their hydrolysis products in water *Surface-Enhanced Raman Scattering* (*Topics in Applied Physics* vol 103) (Berlin: Springer) pp 447–60

[17] Netti M C, Coyle S, Baumberg J J, Ghanem M A, Birkin P R, Bartlett P N and Whittaker D M 2001 Confined surface plasmons in gold photonic nanocavities *Adv. Mater.* **13** 1368–70

[18] Coyle S, Netti M C, Baumberg J J, Ghanem M A, Birkin P R, Bartlett P N and Whittaker D M 2001 Confined plasmons in metallic nanocavities *Phys. Rev. Lett.* **87** 176801

[19] Fischer U C and Zingsheim H P 1981 Submicroscopic pattern replication with visible light *J. Vac. Sci. Technol.* **19** 881–5

[20] Fischer U C, Heimel J, Maas H J, Hartig M, Hoeppener S and Fuchs H 2002 Latex bead projection nanopatterns *Surf. Interface Anal.* **33** 75–80

[21] Haynes C L and Van Duyne R P 2001 Nanosphere lithography: a versatile nanofabrication tool for studies of size-dependent nanoparticle optics *J. Phys. Chem.* B **105** 5599–611

[22] Emory S R and Nie S 1997 Near-field surface-enhanced Raman spectroscopy on single silver nanoparticles *Anal. Chem.* **69** 2631

[23] Kneipp K, Wang Y, Kneipp H, Itzkan I, Dasari R R and Feld M S 1996 Population pumping of excited vibrational states by spontaneous surface-enhanced Raman scattering *Phys. Rev. Lett.* **76** 2444

[24] Netti C, Lincoln J and Flinn G 2005 Reliable substrate technology for surface enhanced Raman spectroscopy *Raman Technology for Today's Spectroscopists*

[25] Etchegoin P G and Le Ru E C 2008 A perspective on single molecule SERS: current status and future challenges *Phys. Chem. Chem. Phys.* **10** 6079–89

[26] Bora M, Fasenfest B J, Behymer E M, Chang A S P, Nguyen H T, Britten J A, Larson C C, Chan J and Bond T C 2010 Plasmon resonant cavities in vertical nanowire array *Nano Lett.* **10** 2832–7

[27] Stockman M I 2004 Nanofocusing of optical energy in tapered plasmonic waveguides *Phys. Rev. Lett.* **93** 137404–1

[28] Gramotnev D K, Vogel M W and Stockman M I 2008 Optimized nonadiabatic nanofocusing of plasmons by tapered metal rods *J. Appl. Phys.* **104** 034311

[29] Gui J Y, Stern A, Frank D G, Lu F, Zapien D C and Hubbard A T 1991 Adsorption and surface structural chemistry of thiophenol, benzyl mercaptan, and alkyl mercaptans. comparative studies at Ag(111) and Pt(111) electrodes by means of auger spectroscopy, electron energy

loss spectroscopy, low-energy electron diffraction, and electrochemistry *Langmuir* **7** 955
[30] Kang H, Park T, Choi I, Lee Y, Ito E, Hara M and Noh J 2009 Formation of large ordered domains in benzenethiol self-assembled monolayers on Au(111) observed by scanning tunneling microscopy *Ultramicroscopy* **109** 1011–4
[31] Fernandez A, Nguyen H T, Britten J A, Boyd R D, Perry M D, Kania D R and Hawryluk A M 1997 Use of interference lithography to pattern arrays of submicron resist structures for field emission flat panel displays *J. Vac. Sci. Technol.* B **15** 729
[32] Aggarwal R L, Farrar L W, Diebold E D and Polla D L 2009 Measurement of the absolute Raman scattering cross section of the 1584 cm^{-1} band of benzenethiol and the surface-enhanced Raman scattering cross section enhancement factor for femtosecond laser-nanostructured substrates *J. Raman Spectrosc.* **40** 1331
[33] Joo T H, Soo M and Kim K 1987 Surface-enhanced Raman scattering of benzenethiol in silver sol *J. Raman Spectrosc.* **18** 57
[34] Lin-Vien D, Colthup N B, Fateley W G and Grasselli J G 1991 *The Handbook of Infrared and Raman Characteristic Frequencies of Organic Molecules* (New York: Academic)
[35] Varsanyi G 1969 *Vibrational Spectra of Benzene Derivatives* (New York: Academic)
[36] Wan L J, Terashima M, Noda H and Osawa M 2000 Molecular orientation and ordered structure of benzenethiol adsorbed on gold (111) *J. Phys. Chem.* B **104** 3563–9
[37] Camon K T and Hurley L G 1991 Axial and azimuthal angle determination with surface-enhanced Raman spectroscopy: thiophenol on copper, silver, and gold metal surfaces *J. Phys. Chem.* **95** 9979–84
[38] Lee S J and Kim K 2003 Development of silver film via thermal decomposition of layered silver alkanecarboxylates for surface-enhanced Raman spectroscopy *Chem. Commun.* **2** 212–213
[39] Mathias S, Carvalho F E and Cecchini E G 1961 The dipole moments of cyclohexanethiol, a-toluenethiol and benzenethiol *J. Phys. Chem.* **65** 425
[40] Bailoa E and Deckert V 2008 Tip-enhanced Raman scattering *Chem. Soc. Rev.* **37** 921–30
[41] Recee P J 2008 Finer optical tweezers *Nat. Photon.* **2** 333–4
[42] Grigorenko A N, Roberts N W, Dickinson M R and Zhang Y 2008 Nanometric optical tweezers based on nanostructured substrates *Nat. Photon.* **2** 365–370
[43] Le Ru E C and Etchegoin P G 2009 *Principles of Surface Enhanced Raman Spectroscopy* (Amsterdam: Elsevier)